

E. J. Crampin · E. A. Gaffney · P. K. Maini

Mode-doubling and tripling in reaction-diffusion patterns on growing domains: A piecewise linear model

Received: 19 December 2000 / Revised version: 24 May 2001 /
Published online: 7 December 2001 – © Springer-Verlag 2001

Abstract. Reaction-diffusion equations are ubiquitous as models of biological pattern formation. In a recent paper [4] we have shown that incorporation of domain growth in a reaction-diffusion model generates a sequence of quasi-steady patterns and can provide a mechanism for increased reliability of pattern selection. In this paper we analyse the model to examine the transitions between patterns in the sequence. Introducing a piecewise linear approximation we find closed form approximate solutions for steady-state patterns by exploiting a small parameter, the ratio of diffusivities, in a singular perturbation expansion. We consider the existence of these steady-state solutions as a parameter related to the domain length is varied and predict the point at which the solution ceases to exist, which we identify with the onset of transition between patterns for the sequence generated on the growing domain. Applying these results to the model in one spatial dimension we are able to predict the mechanism and timing of transitions between quasi-steady patterns in the sequence. We also highlight a novel sequence behaviour, mode-tripling, which is a consequence of a symmetry in the reaction term of the reaction-diffusion system.

1. Introduction

Recent experimental observations on the skin pigmentation of certain species of fish have shown that patterns evolve in a dynamic manner during the growth of the developing animal. Kondo and Asai [15] describe observations on the marine angelfish *Pomacanthus semicirculatus*, where juveniles display a regular array of vertical stripes which increase in number during growth, with new stripes appearing in the gaps between existing ones as the animal doubles in length. This experimentally observed pattern evolution also arises naturally in the reaction-diffusion mechanism with underlying domain growth. These results have sparked renewed interest in reaction-diffusion models for biological pattern formation and, in particular, the role that domain growth may play in the pattern formation mechanism [34, 26, 2]. A specific feature of reaction-diffusion patterns on growing domains is the tendency for stripe patterns to double in the number of stripes each time the domain doubles in

E.J. Crampin, P.K. Maini: Centre for Mathematical Biology, Mathematical Institute, University of Oxford, 24–29 St Giles', Oxford OX1 3LB, UK
e-mail: crampin@maths.ox.ac.uk

E.A. Gaffney: Department of Mathematics and Statistics, University of Birmingham, Edgbaston, Birmingham B15 2TT, UK

Key words or phrases: Reaction-diffusion – Turing system – Pattern formation – Growing domain – Frequency-doubling – Matched asymptotic expansion

length, called mode-doubling. This appears to be a general result for a wide variety of reaction-diffusion models with different reaction kinetics. We have suggested that this mechanism can improve the reliability (robustness) of obtaining specific patterns with many spatial oscillations by growing the pattern up from an initially simple one on an initially small domain [4]. In a one-dimensional system which has been nondimensionalised to the unit interval this phenomenon has been called spatial *frequency*-doubling, and the behaviour was explored in our recent paper (see also [17, 1]). Numerical simulation of reaction-diffusion models with different reaction kinetics demonstrates that frequency-doubling occurs through either the *splitting* and separation of peaks in activator concentration, or by the appearance of new activator peaks at the sites of concentration minima in the previous pattern, which is called peak *insertion*. However, how the mechanism of transition is determined by the reaction kinetics has been unclear.

In this paper we present an analysis of the model for reaction and diffusion on growing domains in one space dimension that was developed in [4], where growth is much slower than the rates of the reaction and diffusion processes. We examine the generation of Turing patterns of large amplitude, far from the bifurcation from the homogeneous steady state. In particular we examine the onset of dynamic transitions between patterns as the domain grows, and establish the factors which determine the mechanism of transition: whether by peak splitting or insertion. Also we find that under certain circumstances both mechanisms may operate simultaneously and a new pattern sequence, spatial *frequency-tripling*, is realised.

We will concentrate on transition-layer-type patterns, consisting of regions of alternating high (peak) and low (trough) value. The width of the transition-layer region decreases as the ratio of diffusivities tends to zero, while the width of the peak (and the spatial location of the transition-layer) remains unaltered. Much of the theory of transition-layers in reaction-diffusion systems was developed by Fife [9]. We will consider monostable systems where there is a single homogeneous steady state which loses stability to a branch of Turing pattern solutions at a critical point. The analysis is simplified by introducing a piecewise linear term for the nonlinear reaction kinetics; an approximation which does not qualitatively affect the solution behaviour. Solutions are analysed in the asymptotic limit as the ratio of diffusivities tends to zero, allowing prediction of the mechanism and timing of dynamic transitions between patterns in a pattern sequence, driven by the domain growth.

2. The model: reaction and diffusion on growing domains

Following Crampin *et al.* [4] the concentration of a chemical species $u(x, t)$ reacting in and diffusing through a growing one-dimensional domain $x \in \Omega(t)$, where time $t \in [0, \infty)$, is governed by the evolution equation

$$u_t + (au)_x = \omega^{-1} D_u u_{xx} + R(u, v, \dots) \quad (1)$$

where R describes reaction with a set of chemicals (u, v, \dots) . We have scaled the equations with a reaction rate ω which is characteristic of the reaction kinetics such that the timescale for pattern formation in the absence of domain growth is $\mathcal{O}(1)$. This equation arises from a kinematic description of domain growth, and

produces two additional terms to the standard reaction diffusion model: a convection term au_x and a dilution term a_xu due to local volume increase. Rather than pose constitutive relations describing the mechanical properties of biological tissue for a particular case, we consider a general framework in which the local flow rate $a(x, t)$ is determined by the local rate of volumetric expansion (strain rate) which we impose on the system, and hence the domain growth may be defined by local (*i.e.* cellular) processes only [3, 6]. In the case of growth at constant strain rate [16] (where all cells in the tissue may be thought of as proliferating at a constant rate) the domain growth is spatially uniform and exponential in time and is described by

$$x = X \exp(\rho t) \quad (2)$$

where X is the Lagrangian (initial) position and ρ is the strain rate.

For this uniform growth the dilution term $a_xu = \rho u$, and by transforming the domain to the unit interval we eliminate the advection term $au_x = \rho xu_x$. For the interaction of two chemical species, and ordering the species with decreasing diffusivity (with long-range inhibitor u and short-range activator v), we recover the nonautonomous system

$$u_t = \gamma^{-1}u_{xx} + f(u, v) - \rho u \quad (3)$$

$$v_t = \varepsilon^2 \gamma^{-1}v_{xx} + g(u, v) - \rho v \quad (4)$$

$$\gamma_t = 2\rho\gamma_0 \exp(2\rho t) \quad (5)$$

defined on

$$x \in [0, 1], \quad t \in [0, \infty) \quad (6)$$

where f and g are the reaction kinetics in a well-stirred medium and $\varepsilon^2 = D_v/D_u$ is the ratio of diffusivities. $\gamma(t)$ is a time-dependent scaling parameter which is proportional to the square of the domain length. Thus for uniform domain growth the model reduces to a reaction-diffusion system with time-dependent diffusivity.

Typically in such models the ratio of diffusivities $\varepsilon^2 = D_v/D_u$ is taken to be small. In [4] we found that pattern sequences are formed under the assumption of *slow* domain growth. This is a natural assumption to make for biological systems, where the reaction and diffusion of chemicals will take place on a timescale much faster than the timescale on which cellular machinery required for tissue growth will operate. We have scaled the equations with a reaction rate ω so that pattern formation takes place on a timescale of $\mathcal{O}(1)$. The timescale characterising domain growth is ρ^{-1} , and so for slow growth we have two small parameters in the problem

$$0 < \rho \ll 1 \quad \text{and} \quad 0 < \varepsilon \ll 1. \quad (7)$$

To close the problem we impose zero flux conditions at the domain boundary which further restricts the pattern behaviour (although zero flux conditions are not a necessary requirement for the frequency-doubling phenomenon):

$$u_x = v_x = 0 \quad \text{on} \quad x = 0, 1. \quad (8)$$

Initial conditions are random perturbations about the homogeneous steady state of the kinetics, (u_s, v_s) where

$$f(u_s, v_s) = g(u_s, v_s) = 0. \quad (9)$$

The initial domain length is contained in the time-zero scaling parameter $\gamma_0 = \omega L_0^2/D_u$ and standard bifurcation techniques show that there is a critical value of γ corresponding to a minimum domain length requirement for pattern formation [5].

In our previous paper [4] we showed that the solutions to this system consist of sequences of quasi-steady patterns (standing waves), after initial transients and for $\gamma > \gamma_c$, with rapid transitions between quasi-steady patterns (pattern reorganisation). The system has two timescales, a slow timescale $\tau = \rho t$ and a fast timescale t . We analyse the system in the asymptotic limit $\rho \rightarrow 0$. Then where $u_\tau, v_\tau \ll \mathcal{O}(\rho^{-1})$ we have the slow system

$$0 = u_{xx} + \gamma f \quad (10)$$

$$0 = \varepsilon^2 v_{xx} + \gamma g \quad (11)$$

$$\gamma(\tau) = \gamma_0 \exp(2\tau) \quad (12)$$

for which quasi-steady solutions to the fixed domain problem are parameterised by γ . The slow system holds except where $u_\tau, v_\tau \sim \mathcal{O}(\rho^{-1})$ for which we have the fast system,

$$u_t = \gamma^{-1} u_{xx} + f \quad (13)$$

$$v_t = \varepsilon^2 \gamma^{-1} v_{xx} + g \quad (14)$$

where on the fast timescale γ is constant, which governs the reorganisation of patterns away from the quasi-steady regime. We note that the dilution term does not appear in either of these expressions and so is safely neglected in the limit $\rho \rightarrow 0$.

Previously we investigated the pattern sequences generated under different functional forms of $\gamma(t)$ corresponding to different schemes for the domain growth. In particular we were interested in the robust generation of pattern: reliable and repeatable pattern formation that is not strongly sensitive to the initial conditions, model parameters and functional form of the kinetics. Under certain conditions on the domain growth the evolution equations generate a regular doubling of the spatial frequency of the quasi-steady standing wave pattern. We found that the incorporation of domain growth was a mechanism for robust pattern formation through the generation of a mode-doubling sequence. Robustness implies that for a large set of initial conditions the same pattern sequence is generated, such that at any time subsequent to initial transients the solution is approximately the same and is independent of the initial conditions, provided that the initial conditions admit the initial Turing bifurcation. It is easier to select patterns at low modes with the equation parameters, and so this presents a mechanism for generating patterns of high spatial mode reliably. In particular, if the initial domain length is below the critical domain length for Turing bifurcation then provided that the initial conditions admit growth of the first mode the sequence of modes 1,2,4,8 . . . will be generated.

In the rest of this paper we investigate the parameterisation by γ of solutions in the slow regime where patterns are in the quasi-steady state. Our method is to exploit the small parameter ε to construct solutions to the steady-state reaction-diffusion system in the limit $\varepsilon \rightarrow 0$ (see for example the books by Grindrod [12] and Kerner and Osipov [14]), and from this to show that the slow dynamics carry the system to a point where the quasi-steady solution ceases to exist, at which point reorganisation of the pattern ensues in the fast regime. The analysis is limited to the slow dynamics, but the identification of mechanisms of reorganisation arises naturally. The analysis predicts the value of γ (and hence the point in time) and the mechanism by which reorganisation proceeds, and how this is determined by the reaction term $R(u, v)$ in the equations.

3. Reaction kinetics

Various schemes have been proposed in the literature as models of biochemical reactions with the prerequisites for the Turing bifurcation in a reaction-diffusion system. We will consider a reaction scheme of polynomial type, and seek to understand the influence of the nonlinearities on sequence formation. We will consider the role that cubic and quadratic nonlinearities play in pattern formation and, in particular, in the transitions between patterns. Ermentrout [8] studied a similar model to investigate the role of the nonlinear kinetics in the selection of spotted and striped patterns on the square two-dimensional domain. It is expedient to expand the kinetic function about the steady state, so that the order of different terms is established. For two interacting species, writing $\mathbf{c} = (\bar{u}, \bar{v}) = (u - u_s, v - v_s)$, any kinetic function R may be expanded as

$$R(\mathbf{c}) = \mathcal{A}\mathbf{c} + \mathcal{N}(\mathbf{c}) \quad (15)$$

$$= \mathcal{A}\mathbf{c} + \mathcal{N}_2(\mathbf{c}, \mathbf{c}) + \mathcal{N}_3(\mathbf{c}, \mathbf{c}, \mathbf{c}) + \dots \quad (16)$$

and we will assume that f and g can be expanded in this way. In what follows we will drop the over-bars on the variables (for notational convenience), noting that we no longer expect everywhere-positive solutions for $\mathbf{c}(x, t)$.

For kinetic terms written in this form, the linearized equation contains simply the Jacobian \mathcal{A} , which should satisfy the conditions for Turing bifurcation (see, for example, the book by Murray [22]). The nonlinearities \mathcal{N}_2 and \mathcal{N}_3 are respectively quadratic and cubic combinations of the concentrations, and no higher nonlinearities will be considered as these are the highest order terms associated with kinetics such as the Schnakenberg [32], glycolysis [33] and Gray-Scott [11] models. The problem may be simplified further by considering only nonlinearities in v , appearing only in the activator equation, such that $f(u, v)$ is linear in u and v . We show later that such a situation can give rise to Turing bifurcation to finite amplitude pattern, and that a sequence of patterns may form on the growing domain as normal. More complicated functional forms for $f(u, v)$ may be considered, but do not qualitatively change the solution behaviour. We will be interested in reaction terms which consist solely of odd powers of the dependent variables such that the reaction-diffusion system is invariant under the parity transformation

$$(u, v) \rightarrow (-u, -v) \quad (17)$$

which is clearly broken by the presence of quadratic terms. Therefore we choose to study a kinetic system with cubic nonlinearity, and then investigate the effect of adding a small quadratic contribution to the reaction term. We stress that we have transformed the equations from the physically significant variables so that the kinetic steady state is at the origin. This simplifies the subsequent analysis. The aim of the analysis is to demonstrate the manner in which the reaction kinetics determine the mechanism of pattern transitions and for this reason it is expedient to consider the symmetric problem, and perturbations which break this symmetry.

The linear part of the reaction term can be chosen to admit the Turing bifurcation, and we can specify the relative polarities of the spatial profiles for activator and inhibitor species according to the signs of the entries in the matrix \mathcal{A} (see for example Dillon *et al.* [5]). We choose a *pure* kinetic system, in which the Fourier modes destabilising the spatially homogeneous state are spatially in phase for the activator and inhibitor. *Cross* kinetics, for which the spatial oscillations are out of phase for the two species, may be studied in the same way, and the analysis is little changed. The general nonlinear kinetic system that we study is given by f and g where

$$f(u, v) = -\sigma u + v \quad (18)$$

$$g(u, v) = -u + \mu v + Qv^2 - v^3 \quad (19)$$

for which the positive constants σ and μ are such that the linearized system with Jacobian matrix

$$\mathcal{A} = \begin{pmatrix} -\sigma & 1 \\ -1 & \mu \end{pmatrix} \quad (20)$$

admits the Turing bifurcation. With suitable rescaling of u , v and time t any pure kinetic scheme may be transformed such that it has a Jacobian of the above form. We will investigate the effect of quadratic terms on the behaviour of a predominantly cubic system by introducing a small quadratic contribution, $|Q| \ll 1$.

Now assuming that f and g are $\mathcal{O}(1)$ it is straightforward to show that the steady-state equations contain two distinct spatial scales. In the asymptotic limit $\varepsilon \rightarrow 0$ we have

$$u_{xx} = -\gamma f(u, v) \quad (21)$$

$$0 = g(u, v) \quad (22)$$

which is the outer subsystem, and rescaling in the inner variable $\xi = x/\varepsilon$ we recover the inner subsystem

$$u_{\xi\xi} = 0 \quad (23)$$

$$v_{\xi\xi} = -\gamma g(u, v) \quad (24)$$

which determines the transition layer, which in the limit has zero width. We study matched solutions of the outer and inner subsystems in the singular limit. In fact the leading order expressions are sufficient for our purposes.

The form of the activator nullcline $g(u, v) = 0$ is critical in determining the solution behaviour in the outer region which, for the nullcline in nonlinear system (19), is cubic in v . In fact the nonlinearities in the equations are such that in practice this is a nontrivial exercise. The inner equations can be integrated, but in the outer solution v is substituted with the root of a cubic and in general a closed form solution cannot be found. However, the essential features of the kinetic system are well approximated by taking a piecewise linear approximation to the reaction term (see for example Rinzel and Keller [31], where a piecewise linear scheme is used to study travelling wave solutions to the FitzHugh-Nagumo model for nerve conduction).

4. Piecewise linear approximation

We introduce a piecewise linear scheme which retains the qualitative features of the nullclines for the nonlinear system. Piecewise linear kinetics are defined such that for the case $Q = 0$ the turning points in the v -nullcline coincide with those for the full nonlinear problem. If we insist that the steady state of the kinetics is at the origin $(0, 0)$ so that the linearized system is simply the linear part of the kinetics, then the nullcline must pass through the origin, where for simplicity we want the kinetics to be continuous. Therefore we approximate the nullcline by three linear regions. We will simulate the effect of introducing a non-zero quadratic contribution by removing the symmetry of the nullcline, as will be shown in detail later. Also in general the gradient of the nullcline can be different in each of the linear regions, but to preserve the symmetry we take equal gradients modulo their sign. The piecewise linear reaction term is

$$f(u, v) = -\sigma u + v \quad (25)$$

$$g(u, v) = g_i = \begin{cases} g_1 & \begin{cases} -u - \eta(v + 2\theta_1), & v < -\theta_1 \\ -u + \eta v, & -\theta_1 \leq v \leq \theta_3 \\ -u - \eta(v - 2\theta_3), & v > \theta_3 \end{cases} \end{cases} \quad (26)$$

where $i = 1, 2, 3$ define the three branches of the g nullcline, dividing (u, v) space into 3 regions at the turning points where $v = -\theta_1$ and $v = \theta_3$ respectively, for positive constants θ_1 and θ_3 . We will use subscripts to refer to these three regions. The piecewise linear kinetics are such that the reaction term is continuous at $v = -\theta_1$ and $v = \theta_3$ for all u . In order that the turning points for the nonlinear and piecewise linear kinetics coincide we modify one of the parameters in the linearized equations, taking

$$\eta = \frac{2}{3}\mu. \quad (27)$$

This does not qualitatively alter the behaviour of the equations. The manner in which the turning points depend continuously on Q for the full nonlinear problem is approximated by taking

$$\theta_{1,3} = \frac{1}{3} \left(\sqrt{3\mu + Q^2} \mp Q \right). \quad (28)$$

We have chosen parameters such that the Turing bifurcation is still admitted in the linearized system with Jacobian

$$\mathcal{A} = \begin{pmatrix} -\sigma & 1 \\ -1 & \eta \end{pmatrix}. \quad (29)$$

Solutions to evolution equations (3–5) for the activator species, $v(x, t)$, with nonlinear kinetics (18–19) and for the piecewise linear scheme (25–26) are compared in Fig. 1. In the figure the three sequence types are illustrated: frequency-doubling by peak splitting (a), (b) and peak insertion (e), (f), and frequency-tripling (c), (d). The different sequences are achieved according to whether a small quadratic perturbation is added to the cubic kinetics, and according to the sign of the perturbation. For the piecewise linear kinetics the parity symmetry is broken by moving the turning points according to equation (28). In each case the nonlinear and corresponding piecewise linear kinetics can be seen to give qualitatively similar behaviour. Nullclines for this system, given by

$$f(u, v) = 0, \quad u = \frac{1}{\sigma}v \quad (30)$$

$$g(u, v) = 0, \quad u = \begin{cases} -\eta(v + 2\theta_1), & v < -\theta_1 \\ \eta v, & -\theta_1 \leq v \leq \theta_3 \\ -\eta(v - 2\theta_3), & v > \theta_3 \end{cases} \quad (31)$$

are drawn in Fig. 2 for the symmetric case $Q = 0$ and for an example where $Q \neq 0$, and we have superimposed the g nullcline for the full nonlinear system (19).

The linear system that we study may, naturally, be solved exactly in each of the linear regions of the reaction term, and the undetermined constants eliminated by patching these solution segments together appropriately. However, such an undertaking is algebraically challenging, sufficiently so to obscure the insights to be gained from the simplifying approximation we have made, and indeed we quickly find that the solution cannot be expressed in closed form. Thus we pursue an asymptotic approximation and consider only the leading order in an expansion in ε .

The outer solution is constrained to lie on the three-branched nullcline $g = 0$. Then locally, and away from the quasi-steady state, we find in the outer approximation

$$v_t = g(u, v) \quad (32)$$

and with the form of g given in (19) it is straightforward to show that branch 2 is unstable to small perturbations in v for all u . Therefore the time-independent (steady state) outer solutions lie on branches 1 and 3, corresponding to low and high v (and u for a pure kinetic system) respectively.

For illustrative purposes we will consider the simplest pattern admitted as a solution of the system: a pattern of lowest mode, and with negative polarity such that there is a single internal transition layer from low to high v across the domain. We locate the internal transition layer at

$$x = x^* \in [0, 1] \quad (33)$$

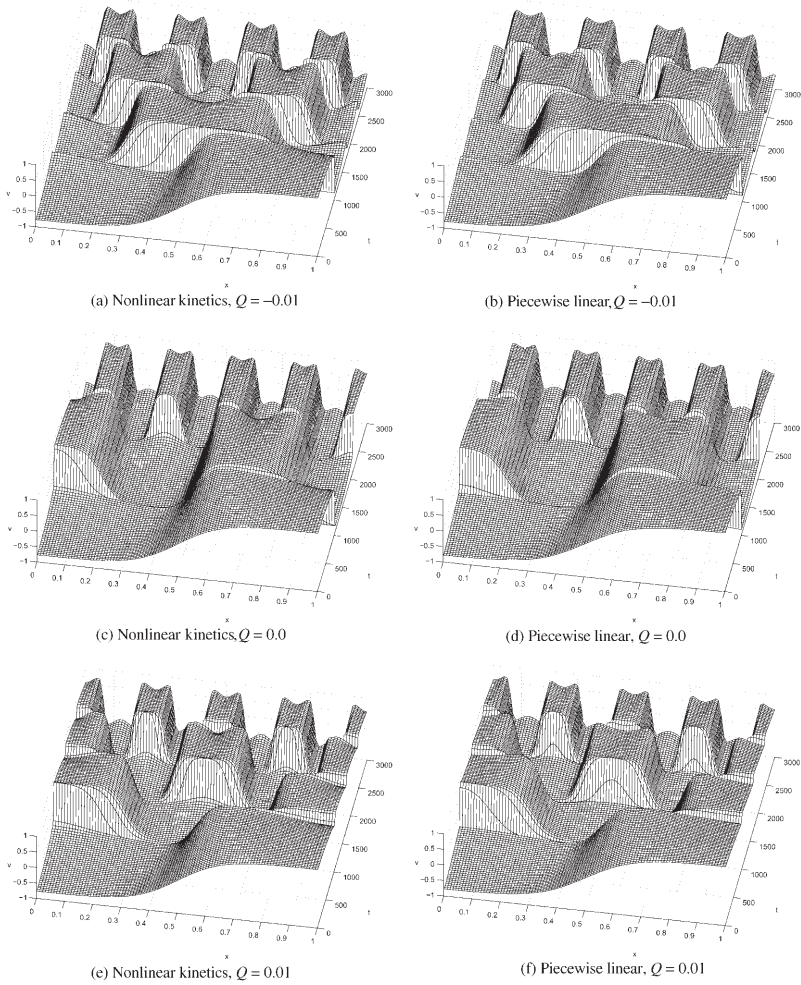


Fig. 1. Numerical solutions to evolution equation (3–5) comparing nonlinear (19) and corresponding piecewise linear (25–26) kinetics for $\varepsilon = 0.1$. Here and elsewhere $\gamma_0 = 1.0$ and $\rho = 0.001$.

which will be determined by the analysis. The inner equation (23) subject to matching constraints gives the inner approximation

$$u(\xi) = u^* \tag{34}$$

where u^* is constant, and hence, trivially, that u is continuous in the inner region.

For the full problem, direct integration of the steady-state inhibitor equation (10) over the domain with boundary conditions (8) gives

$$\int_0^1 f(u, v) dx = 0 \tag{35}$$

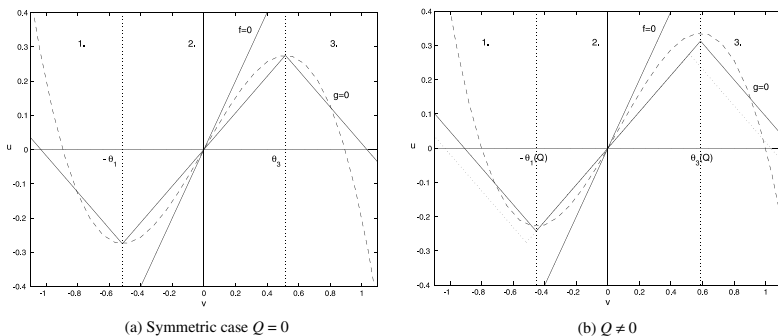


Fig. 2. Nullclines for the piecewise linear kinetic scheme (2). Superimposed are the nullclines for nonlinear cubic autocatalysis (19) (dashed line). In (a) $Q = 0$ and in (b) $Q = 0.2$ (dotted lines showing the symmetric case), with $\sigma = 1.0$ and $\mu = 0.8$ in both.

which we require of our asymptotic solutions, so that the gradient in u is continuous across the inner region. Also the equations admit a first integral and from (11) we have

$$\frac{1}{2} (\varepsilon v_x)^2 + \gamma \int_{v(0)}^{v(x)} g \, dv = 0 \tag{36}$$

so that evaluating over the domain we require

$$\int_{v(0)}^{v(1)} g(u, v) \, dv = 0 \tag{37}$$

where the integrand is zero except in the inner region. Integrating, we find that

$$u^* = \frac{1}{2} \eta (\theta_3 - \theta_1) \tag{38}$$

and we conclude that the value of u in the inner region, u^* , does not depend on γ . We construct solutions such that v and its first derivative are continuous across the inner region. We defer detailed discussion of the construction of solutions to the Appendix. Composite solutions after matching are

$$u(x) \sim a_1 \cosh(\lambda \sqrt{\gamma} x) - \frac{2\theta_1}{\lambda^2}, \quad 0 \leq x < x^* \tag{39}$$

$$\sim a_3 \cosh(\lambda \sqrt{\gamma} (1-x)) + \frac{2\theta_3}{\lambda^2}, \quad x^* \leq x \leq 1 \tag{40}$$

and

$$v(x) \sim -\frac{a_1}{\eta} \cosh(\lambda\sqrt{\gamma}x) + (\theta_1 + \theta_3) \exp\left[\sqrt{\gamma\eta}\left(\frac{x-x^*}{\varepsilon}\right)\right] - \frac{2\sigma\theta_1}{\lambda^2}, \quad 0 \leq x < x^* \quad (41)$$

$$\sim -\frac{a_3}{\eta} \cosh(\lambda\sqrt{\gamma}(1-x)) - (\theta_1 + \theta_3) \exp\left[-\sqrt{\gamma\eta}\left(\frac{x-x^*}{\varepsilon}\right)\right] + \frac{2\sigma\theta_3}{\lambda^2}, \quad x^* \leq x \leq 1 \quad (42)$$

where $\lambda = \sqrt{\sigma + 1/\eta}$, the location of the transition layer $x^*(\gamma)$ is unknown at this stage, and a_1 and a_3 are constants which may depend on x^* and γ . Matching inner and outer solutions gives

$$a_1(x^*) = \frac{1}{\cosh(\lambda\sqrt{\gamma}x^*)} \left(u^* + \frac{2\theta_1}{\lambda^2}\right) \quad (43)$$

$$a_3(x^*) = \frac{1}{\cosh(\lambda\sqrt{\gamma}(1-x^*))} \left(u^* - \frac{2\theta_3}{\lambda^2}\right) \quad (44)$$

where u^* is determined above, and from equation (35) we have

$$a_1 \sinh(\lambda\sqrt{\gamma}x^*) = -a_3 \sinh(\lambda\sqrt{\gamma}(1-x^*)). \quad (45)$$

Now we can find the location of the transition layer $x^*(\gamma)$ from the expressions for constants a_1 and a_3 which gives for $x^*(\gamma)$

$$\bar{\theta}_1 \tanh(\lambda\sqrt{\gamma}x^*) = \bar{\theta}_3 \tanh(\lambda\sqrt{\gamma}(1-x^*)) \quad (46)$$

where we have defined

$$\bar{\theta}_1 \equiv \frac{2\theta_1}{\lambda^2} + u^*, \quad \bar{\theta}_3 \equiv \frac{2\theta_3}{\lambda^2} - u^*. \quad (47)$$

Clearly for the symmetric case $\theta_1 = \theta_3$, $x^* = 1/2$ and the transition layer does not move with γ (and hence domain length), but in general we solve (46) by writing $z = \exp(2\lambda\sqrt{\gamma}x^*)$, rearranging to obtain the quadratic in $z(\gamma)$

$$(\bar{\theta}_1 + \bar{\theta}_3) z^2 + (\bar{\theta}_1 - \bar{\theta}_3) (\exp(2\lambda\sqrt{\gamma}) - 1)z - \exp(2\lambda\sqrt{\gamma}) (\bar{\theta}_1 + \bar{\theta}_3) = 0 \quad (48)$$

and, taking the positive solution z_+ , we find that

$$x^*(\gamma) = \frac{1}{2\lambda\sqrt{\gamma}} \ln z_+ \quad (49)$$

which completes the construction of solutions to the steady-state problem.

In Figs. 3 and 4 we plot steady-state numerical solutions of equations (13–14) and the analytical approximations given by equations (39–42) for both $Q = 0$ and for $Q \neq 0$. The analytical solution is shown to be close to the numerical solution, and the approximation improves as ε decreases.

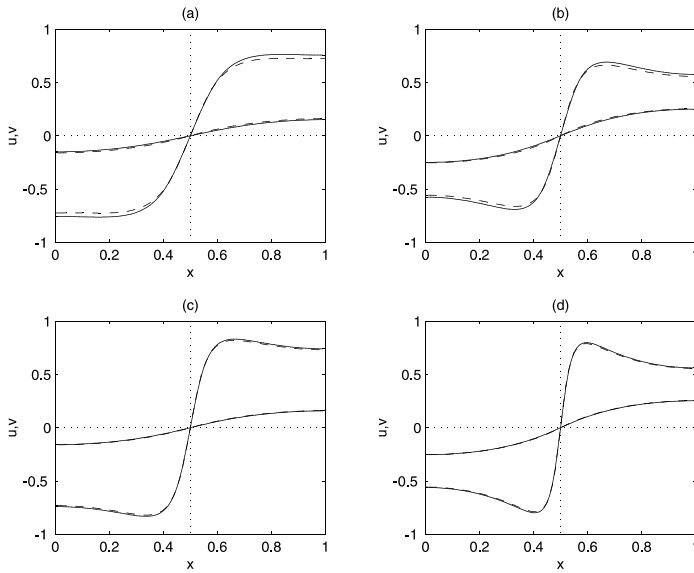


Fig. 3. The symmetric case: numerical solution of equations (3–5) (solid line) and asymptotic approximation (39–42) (dashed line) for piecewise linear kinetic scheme (25–26) with $Q = 0$. Activator solutions (v) are of larger amplitude than inhibitor solutions (u), both are shown. Figures (a) and (b) have $\varepsilon = 0.1$ while (c) and (d) have $\varepsilon = 0.05$. Left-hand figures have $\gamma = 2.0$ and right-hand figures have $\gamma = 6.0$.

5. Transitions between patterns

The construction that we have described above generates an approximation to the true solution of the time-independent problem up to the point at which a pattern of higher mode (higher spatial frequency on $[0, 1]$) is established. However, we can estimate the limit for such construction as γ increases through critical values, which determines the mechanisms of breakdown for the full PDE system.

The outer solution is constrained to lie on the v -nullcline $g = 0$ in regions 1 and 3. The solution evolves with γ until this constraint can no longer be satisfied. As γ is increased the solutions are limited by the turning points of the v nullcline $g = 0$, the critical points

$$v_1^c \equiv -\theta_1, \quad u_1^c \equiv \eta v_1^c = -\eta\theta_1 \quad (50)$$

$$v_3^c \equiv \theta_3, \quad u_3^c \equiv \eta v_3^c = \eta\theta_3 \quad (51)$$

and the solution we have constructed breaks down at these values. For the lowest pattern mode u is monotonic across the domain, and the maximum and minimum occur at the domain boundaries. As γ is further increased, at one of the boundaries u is pushed past the critical value. Splitting or insertion follows (which is not quasi-steady and thus may not be directly studied by this method) depending on which of the critical points (u_1^c, v_1^c) or (u_3^c, v_3^c) is reached first. In the symmetric case, where $\theta_1 = \theta_3$, both the critical points are reached at the same time giving

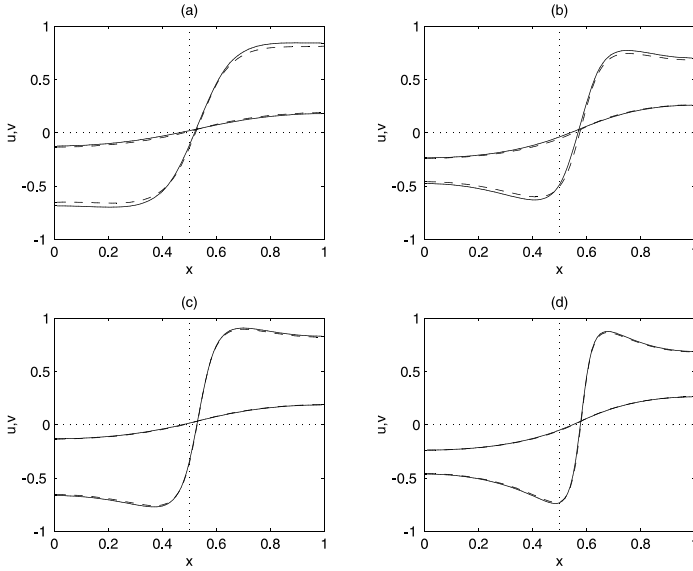


Fig. 4. The asymmetric case: numerical solution of equations (3–5) (solid line) and asymptotic approximation (39–42) (dashed line) for piecewise linear kinetics (25–26) with $Q = 0.2$. Activator solutions (v) are of larger amplitude than inhibitor solutions (u), both are shown. Figures (a) and (b) have $\varepsilon = 0.1$ while (c) and (d) have $\varepsilon = 0.05$. Left-hand figures have $\gamma = 2.0$ and right-hand figures have $\gamma = 5.0$.

rise to simultaneous splitting and insertion, as realised in the numerical simulations showing frequency-tripling (Fig. 1 (c) and (d)). We can use the critical values to predict the value of γ at which the breakdown occurs, and by what mechanism, for specific parameter sets.

Working with u at the domain boundaries, from equations (39, 40) we have

$$u(0) = a_1 - \frac{2\theta_1}{\lambda^2}, \quad u(1) = a_3 + \frac{2\theta_3}{\lambda^2}. \tag{52}$$

Now if $u(0)$ reaches u_1^c at $\gamma = \gamma_1^c$ then substituting for a_1 we have

$$\lambda\sqrt{\gamma}x^* = \cosh^{-1} \left[\frac{\lambda^2\bar{\theta}_1}{2\theta_1 - \eta\lambda^2\theta_1} \right] \equiv \phi_1 \tag{53}$$

where $x^* = x^*(\gamma)$. We substitute this into equation (48) with $z = z_1 = \exp 2\phi_1$ and after some algebra we find

$$\gamma_1^c = \left\{ \frac{1}{2\lambda} \ln \left[\frac{(\bar{\theta}_1 + \bar{\theta}_3)z_1^2 - (\bar{\theta}_1 - \bar{\theta}_3)z_1}{(\bar{\theta}_1 + \bar{\theta}_3) - (\bar{\theta}_1 - \bar{\theta}_3)z_1} \right] \right\}^2. \tag{54}$$

Similarly, if $u(1)$ arrives at u_3^c when $\gamma = \gamma_3^c$ then we have

$$\lambda\sqrt{\gamma}x^* = \cosh^{-1} \left[\frac{\lambda^2\bar{\theta}_3}{2\theta_3 - \eta\lambda^2\theta_3} \right] \equiv \phi_3 \tag{55}$$

from which we have

$$\gamma_3^c = \left\{ \frac{1}{2\lambda} \ln \left[\frac{(\bar{\theta}_1 + \bar{\theta}_3)z_3^2 + (\bar{\theta}_1 - \bar{\theta}_3)z_3}{(\bar{\theta}_1 + \bar{\theta}_3) + (\bar{\theta}_1 - \bar{\theta}_3)z_3} \right] \right\}^2 \tag{56}$$

for $z_3 = \exp 2\phi_3$.

On reaching one (or both) of these critical points, the solution we have constructed ceases to exist. In the outer region where $x < x^*$, and in particular at $x = 0$ we have

$$\frac{du(0)}{d\gamma} < 0 \tag{57}$$

so that the quasi-steady approximation breaks down as $u(0)$ decreases through u_1^c . Then locally $g < 0$ and so $v_t < 0$ and so when $u < u_1^c$, branch 3 of the nullcline $g = 0$ is attracting and the v solution relaxes to this branch on the fast timescale, giving a sudden growth of activator at the boundary (a minimum in the solution profile). This mechanism describes the onset of insertion of new activator peaks, shown schematically in Fig. 5. Similarly at $x = 1$ we find

$$\frac{du(1)}{d\gamma} > 1 \tag{58}$$

and the solution breaks down as $u(1)$ increases through u_3^c . Here $g > 0$ and $v_t > 0$ and the v solution relaxes to branch 1 of the nullcline on the fast timescale giving a sudden collapse at the activator peak, producing dynamic pattern change by activator peak splitting. When the boundary values pass through these critical points at the same value of γ due to the symmetry of the kinetics (when $Q = 0$) both splitting and insertion occur simultaneously.

Analytical predictions and the results of numerical simulations for the piecewise linear kinetics are presented in Fig. 6, where the dashed line shows $\gamma_1^c(Q)$ corresponding to insertion and the dotted line is $\gamma_3^c(Q)$ which corresponds to splitting. We note that both curves extend on each side of $Q = 0$, but in simulations of the full PDE we expect to observe which ever occurs at lower γ^c . In Fig. 7 the

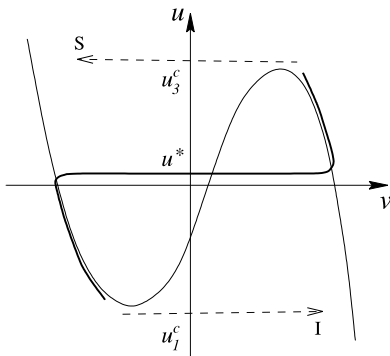


Fig. 5. Schematic diagram illustrating the mechanisms of insertion (I) and splitting (S) of new activator peaks when domain growth (increasing γ) drives the solution in the outer region to the limiting points of the nullcline, (u_1^c, v_1^c) and (u_3^c, v_3^c) respectively.

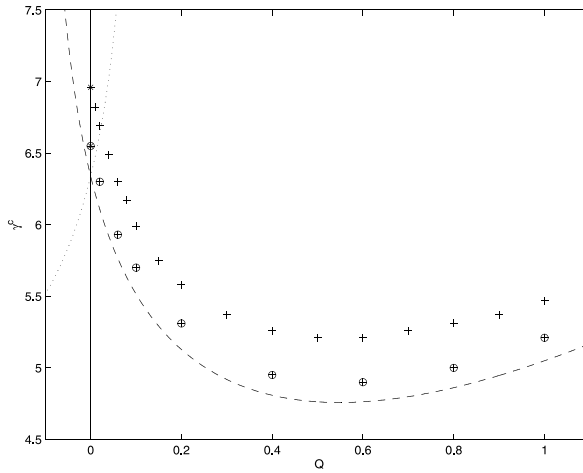


Fig. 6. Analytical prediction of pattern reorganisation by peak insertion, $\gamma_1^c(Q)$ (dashed line), and insertion, $\gamma_3^c(Q)$ (dotted line), given by equations (54) and (56) respectively. The dependence of these values on Q is determined by the dependence of θ_1 and θ_3 given by equation (28). Numerical points for piecewise linear kinetics with $Q \geq 0$ show pattern reorganisation by peak insertion (marked +) and simultaneous splitting and insertion (marked *), and the numerical results are plotted for $\varepsilon = 0.1$ and $\varepsilon = 0.05$ (circled symbols). The transition is between pattern modes 1 and 2.

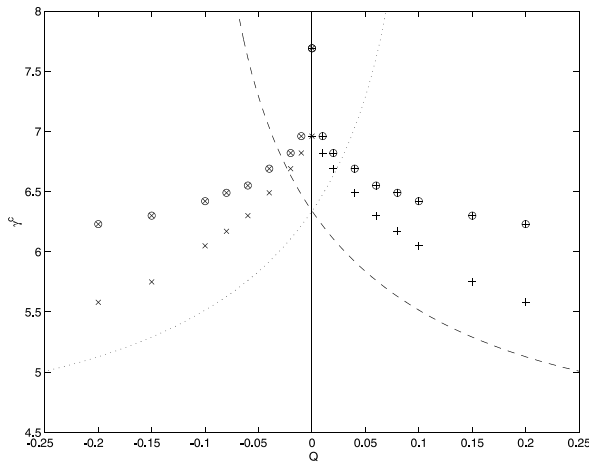


Fig. 7. Analytical predictions for transition points showing numerical results for piecewise linear kinetics and nonlinear kinetics (circled symbols). The dotted line gives the analytical prediction for peak splitting and the dashed line shows the prediction for peak insertion. Numerical points for splitting are marked \times and for insertion $+$. Simultaneous splitting and insertions are marked $*$.

values of γ at which transitions between patterns occur for the full nonlinear system are plotted for small Q , showing qualitatively similar behaviour to the piecewise linear approximation.

6. Discussion

In this paper we have considered a piecewise linear reaction-diffusion model and we have determined the method of pattern reorganisation on the growing domain by considering the existence of solutions to the associated steady-state problem. We have not explicitly considered the stability of the constructed solutions, rather we infer stability properties from numerical simulations. Previous results for the full PDEs suggest that stability depends on domain growth [4], i.e. $\gamma(t)$, in a nontrivial way. For example, linear domain expansion (rather than the exponential case considered above) leads to the breakdown of the frequency-doubling sequence at some particular domain size, when one or more peaks fail to split (or insert) concurrently with others.

Spatial frequency-doubling has been explored previously using symmetry arguments [4]. The domain may be divided into subdomains on each of which the solution evolves identically. Furthermore the solution on each subdomain is the same as the solution on the whole domain at some earlier time, and evolves in the same way as the earlier solution. We used a self-similarity argument: the solution at a particular value of $\gamma = \gamma^*$, transformed under the ‘doubling map’

$$p_2(x) = \begin{cases} 2x, & 0 \leq x < \frac{1}{2} \\ 2(1-x), & \frac{1}{2} \leq x \leq 1 \end{cases} \quad (59)$$

is a solution of the equation at $\gamma = 4\gamma^*$. This result confirms that the pattern will double in frequency when the domain doubles in length (as γ is proportional to the length squared). A similar argument has recently been given by Nishiura and Ueyama [24] to explain a hidden bifurcation structure leading to peak splitting in transient patterns in bistable reaction-diffusion equations on the fixed domain, which they have called *doubling-up*. Here we have described a new pattern sequence, spatial frequency-tripling, which is realised when the reaction-diffusion equation is symmetric under the transformation $(u, v) \rightarrow (-u, -v)$. Then we must amend the symmetry analysis for this new sequence. Accordingly it is straightforward to show that the equation is also invariant under the transformation

$$(x, \gamma) \rightarrow (\bar{p}_3(x), \gamma/9) \quad (60)$$

corresponding to a tripling of the domain length, where the ‘tripling map’ is

$$\bar{p}_3(x) = \begin{cases} 1-3x, & 0 \leq x < \frac{1}{3} \\ 3x-1, & \frac{1}{3} \leq x < \frac{2}{3} \\ 3(1-x), & \frac{2}{3} \leq x \leq 1 \end{cases}. \quad (61)$$

Hence the new sequence is consistent with the symmetry arguments, which are described in more detail in the previous paper. It is interesting to note that the symmetry required for frequency-tripling is the same as that required for preferential selection of stripes over spots in two-dimensional pattern formation in reaction-diffusion systems [8,21].

Our choice of pattern, the simple monotonic gradient for u and corresponding transition layer for v , may first appear to be rather a restricted case. However,

the results are easily generalised to patterns of higher mode using such symmetry arguments as presented above. While we chose to construct a pattern of negative polarity (transition from low to high v with increasing x), the invariance of the reaction-diffusion equations under the transformation $x \rightarrow -x$ shows the equivalence of patterns of opposite polarity. Furthermore, any pattern of higher mode may be constructed from suitably spatially scaled segments consisting of the lowest mode pattern that we constructed above. Also the analysis extends *mutatis mutandis* to the case of cross kinetic schemes, where the spatial oscillations in u and v are out of phase.

The model studied in this paper considers perhaps the simplest possible form of domain growth, where cellular proliferation rates are constant in space and time. We study the effects of domain growth, rather than modelling the mechanics of tissue movement and expansion itself. The formalism used allows consideration of domain growth in higher spatial dimensions and domain growth that is not uniform in space where, for example, the cellular proliferation rate in one part of the tissue is greater than it is elsewhere. The implications of nonuniform domain growth on pattern formation are currently under investigation, however, initial results suggest that gentle gradients in strain rate across the domain do not significantly perturb the behaviour discussed above. Extension of the solution behaviour described here to domains of higher spatial dimension has also been studied; the results will be reported elsewhere. However, in the context of the one-dimensional model, it is important to note that simulations on a two-dimensional growing domain indicate that pattern sequences for stripe patterns may be generated (for reaction kinetics that select stripes in two dimensions, such as those studied here), analogously to the one-dimensional case. Indeed splitting or insertion of stripes during domain growth may be a mechanism for stabilising the orientation of the stripe pattern. This is important for the comparison with the growing angelfish *Pomacanthus semicirculatus*, as discussed in the introduction, where new vertical stripes are inserted as the animal grows concurrently along the antero-posterior (head-to-tail) axis and the dorso-ventral (top-to-bottom) axis. However, it is clear that to fully extend the results to higher spatial dimensions it will be important to consider the effects of curvature and changing geometry of the domain in the model.

Self-replication phenomena similar to peak splitting have been reported in numerical studies of bistable reaction-diffusion systems on domains of *fixed* size in two spatial dimensions (self-replicating spots) [27, 19] and in chemical experiments ([18], reviewed by Lee and Swinney [20]), and related behaviour has been studied in one spatial dimension [28, 29]. The reaction term used in these studies, the Gray-Scott model [11] in the vicinity of the bistable parameter regime, gives rise to spike-type patterns. Spike solutions to reaction-diffusion systems have sharp peaks in the vicinity of one or more spatial points, where the width of the peak tends to zero with the ratio of diffusivities [23, 13]. Self-replication has been investigated analytically in several papers which exploit the ratio of diffusivities as a small parameter [30, 7]. Osipov and Severtsev [25] have used an asymptotic approach for spike solutions and have discussed replication and periodic patterns on infinite domains.

Monostable systems of the type that we consider in this paper do not undergo spontaneous self-replication. However, as we have demonstrated, peak splitting may be driven by domain growth in such systems. The kinetic scheme that we have studied gave rise to transition-layer-type patterns. Spike solutions are also found in systems which do not undergo self-replication phenomena, such as the Schnakenberg [32] and Gierer-Meinhardt [10] models, which have no bistable regime. These systems, which are commonly employed to model biological pattern formation, demonstrate respectively splitting and insertion of activator peaks when driven by domain growth.

Appendix

The outer solutions lie on the nullcline $g = 0$ in regions 1 and 3, the former corresponding to $v < 0$ and the latter to $v > 0$. Choosing to construct a pattern of mode $m = 1$ with negative polarity (corresponding to linear mode $\sqrt{\cdot}(x) = -\cos \pi x$) we take $v < 0$ near $x = 0$. In region 1, $g_1(u, v) = 0$ gives $v = v_1(u)$ and equation (21) becomes

$$u_{xx} - \gamma \lambda^2 u = 2\gamma \theta_1, \quad u_x(0) = 0 \quad (62)$$

with solution

$$u_1(x) = a_1 \cosh(\lambda \sqrt{\gamma} x) - \frac{2\theta_1}{\lambda^2} \quad (63)$$

where

$$\lambda \equiv \sqrt{\sigma + \frac{1}{\eta}}. \quad (64)$$

Similarly in region 3, where the nullcline $g_3(u, v) = 0$ gives $v = v_3(u)$ we have

$$u_3(x) = a_3 \cosh(\lambda \sqrt{\gamma}(1-x)) + \frac{2\theta_3}{\lambda^2}. \quad (65)$$

These equations also determine the activator profiles in the outer regions through the relations $g_i(u_i, v_i) = 0$ with $i = 1, 3$, giving

$$v_1(x) = -\frac{a_1}{\eta} \cosh(\lambda \sqrt{\gamma} x) - \frac{2\sigma \theta_1}{\lambda^2} \quad (66)$$

$$v_3(x) = -\frac{a_3}{\eta} \cosh(\lambda \sqrt{\gamma}(1-x)) + \frac{2\sigma \theta_3}{\lambda^2}. \quad (67)$$

The transition layer is determined by the inner approximation from equation (23), where we take u constant in the inner variable. This is the only possibility admitted by the equations given that the inner solution must decay (or at least not grow) away from x^* to match the outer solution in regions 1 and 3. For the inner solution (U, V) we have

$$U = u^* \quad (68)$$

which is determined by integral condition (37)

$$\int_{v(0)}^{v(1)} g(u, v) dv = 0, \quad (69)$$

which we can divide into regions, yielding outer and inner contributions, giving

$$u^* = \frac{1}{2}\eta(\theta_3 - \theta_1) \quad (70)$$

and so we find that the value of u in the inner region does not depend on γ . We note that u^* is located symmetrically between the extrema $u_1^c = -\eta\theta_1$ and $u_3^c = \eta\theta_3$, such that at $x = x^*$ we have $v = (\theta_3 - \theta_1)/2$.

The inner equation, $V_{\xi\xi} = -\gamma g(u^*, V)$ with $V_{\xi} \rightarrow 0$ as $\xi \rightarrow \pm\infty$, has translational invariance, and so $V(\xi + \alpha)$ is a solution for arbitrary constant α . Therefore we define the transition x^* to be the point where V_{ξ} takes its maximum value. Construction of the inner solution for V is complicated by the fact that we must patch together solutions for regions $i = 1, 2$ and 3 , where we require continuity of the inner solution for V when the kinetics change abruptly at $V = -\theta_1$ and again at $V = \theta_3$. With inner variable $\xi = (x - x^*)/\varepsilon$, for region 1 where $g = g_1(u^*, V)$ we have

$$V_{\xi\xi} - \gamma\eta V = \frac{1}{2}\gamma\eta(3\theta_1 + \theta_3) \quad (71)$$

and we take the solution which decays as $\xi \rightarrow -\infty$

$$V_1(\xi) = b_1 \exp(\sqrt{\gamma\eta}\xi) - \frac{1}{2}(3\theta_1 + \theta_3). \quad (72)$$

Similarly in region 3 we find

$$V_3(\xi) = b_3 \exp(-\sqrt{\gamma\eta}\xi) + \frac{1}{2}(\theta_1 + 3\theta_3) \quad (73)$$

which decays as $\xi \rightarrow \infty$. In region 2 the inner solution satisfies

$$V_{\xi\xi} + \gamma\eta V = \frac{1}{2}\gamma\eta(\theta_3 - \theta_1) \quad (74)$$

which gives

$$V_2(\xi) = b_2 \sin(\sqrt{\gamma\eta}\xi + \alpha) + \frac{1}{2}(\theta_3 - \theta_1) \quad (75)$$

where b_1 , b_2 and b_3 are constants. The transition point, where $x = x^*$, occurs within region 2 and so at $\xi = 0$ we impose $V_{\xi} = 0$ to find $\alpha = 0$. We require that the inner solution and derivative are continuous where the nullclines change between regions 1 and 2 at $V = -\theta_1$ and between regions 2 and 3 at $V = \theta_3$, where $\xi = \xi_{12}$ and ξ_{23} respectively, giving

$$\xi_{12} = \frac{-\pi}{4\sqrt{\gamma\eta}}, \quad \xi_{23} = \frac{\pi}{4\sqrt{\gamma\eta}} \quad (76)$$

and

$$b_1 = \frac{1}{2} (\theta_1 + \theta_3) \exp(-\pi/4) \quad (77)$$

$$b_2 = \frac{1}{\sqrt{2}} (\theta_1 + \theta_3) \quad (78)$$

$$b_3 = -\frac{1}{2} (\theta_1 + \theta_3) \exp(\pi/4). \quad (79)$$

The resulting expression for $v(x)$ is somewhat cumbersome, however, we notice that by neglecting the inner solution in region 2 and considering the solutions in region 1 and 3 only, we do not change the matching condition for the leading order calculation and retain a good approximation to the numerical solution (see Figs. 3 and 4). Then requiring continuity of the inner solution and its derivative at $\xi = 0$ we can find the constants b_1 and b_3 ,

$$b_1 = -b_3 = (\theta_1 + \theta_3). \quad (80)$$

Explicit computation readily shows that the maximum *absolute* error in region 2 associated with the above approximation is $(\theta_1 + \theta_3) (1/2 - \exp(-\pi/4)) \approx 0.04 (\theta_1 + \theta_3)$, and this along with the maximum *relative* error in regions 1 and 3 introduced by neglecting region 2 is sufficiently small for our purposes.

To match inner and outer approximations we require

$$u^* = a_1 \cosh(\lambda\sqrt{\gamma}x^*) - \frac{2\theta_1}{\lambda^2} \quad (81)$$

and

$$u^* = a_3 \cosh(\lambda\sqrt{\gamma}(1-x^*)) + \frac{2\theta_3}{\lambda^2} \quad (82)$$

from which we recover equations (43) and (44). The final condition that we require to calculate the location of the transition layer, x^* , comes from integral condition (35)

$$\int_0^1 f(u, v) dx = 0 \quad (83)$$

which gives

$$a_1 \sinh(\lambda\sqrt{\gamma}x^*) = -a_3 \sinh(\lambda\sqrt{\gamma}(1-x^*)) \quad (84)$$

and is equivalent to the requirement that the gradient in the outer region be continuous at x^* . This completes the construction of the leading order solutions.

Acknowledgements. EJC acknowledges an earmarked studentship from the BBSRC. EAG was supported by a Wellcome Trust postdoctoral fellowship.

References

1. Arcuri, P., Murray, J.D.: Pattern sensitivity to boundary and initial conditions in reaction-diffusion models, *J. Math. Biol.*, **24**: 141–165 (1986)
2. Chaplain, M.A.J., Ganesh, M., Graham, I.G.: Spatio-temporal pattern formation on spherical surfaces: Numerical simulation and application to solid tumour growth, *J. Math. Biol.*, **42**(5): 387–423 (2001)
3. Crampin, E.J.: *Reaction-diffusion patterns on growing domains*, D. Phil. Thesis., University of Oxford, (2000)
4. Crampin, E.J., Gaffney, E.A., Maini, P.K.: Pattern formation through reaction and diffusion on growing domains: Scenarios for robust pattern formation, *Bull. Math. Biol.*, **61**: 1093–1120 (1999)
5. Dillon, R., Maini, P.K., Othmer, H.G.: Pattern formation in generalized Turing systems I: Steady-state patterns in systems with mixed boundary conditions, *J. Math. Biol.*, **32**(4): 345–393 (1994)
6. Dillon, R., Othmer, H.G.: A mathematical model for outgrowth and spatial patterning of the vertebrate limb bud, *J. theor. Biol.*, **197**: 295–330 (1999)
7. Doelman, A., Kaper, T.J., Zegeling, P.A.: Pattern formation in the one-dimensional Gray-Scott model, *Nonlinearity*, **10**: 523–563 (1997)
8. Ermentrout, B.: Spots or stripes? Nonlinear effects in bifurcation of reaction-diffusion equations on the square, *Proc. R. Soc. Lond. A.*, **434**: 413–417 (1991)
9. Fife, P.C.: Stationary patterns for reaction-diffusion equations, In Fitzgibbon III, W.E., Walker, H.F., editors, *Nonlinear Diffusion*, Research Notes in Mathematics 14, pages 81–121. Pitman, London, (1977)
10. Gierer, A., Meinhardt, H.: A theory of biological pattern formation, *Kybernetik*, **12**: 30–39 (1972)
11. Gray, P., Scott, S.K.: Autocatalytic reactions in the isothermal, continuous stirred tank reactor: Oscillations and instabilities in the system $A + 2B \rightarrow 3B$, $B \rightarrow C$, *Chem. Eng. Sci.*, **39**(6): 1087–1097 (1984)
12. Grindrod, P.: *The Theory and Applications of Reaction-Diffusion Equations: Patterns and Waves.*, Oxford University Press, 2nd edition, (1996)
13. Iron, D., Ward, M.J., Wei, J.: The stability of spike solutions to the one-dimensional Gierer-Meinhardt model, *Physica D*, **150**(1–2): 25–62 (2001)
14. Kerner, B.S., Osipov, V.V.: *Autosolitons: A New Approach to the Problem of Self-Organisation and Turbulence*, Kluwer, Dordrecht, (1994)
15. Kondo, S., Asai, R.: A reaction-diffusion wave on the skin of the marine angelfish *Pomacanthus*, *Nature*, **376**: 765–768 (1995)
16. Kulesa, P.M., Cruywagen, G.C., Lubkin, S.R., Maini, P.K., Sneyd, J., Ferguson, M.W.J., Murray, J.D.: On a model mechanism for the spatial patterning of teeth primordia in the alligator, *J. theor. Biol.*, **180**: 287–296 (1996)
17. Lacalli, T.C.: Dissipative structures and morphogenetic pattern in unicellular algae, *Phil. Trans. R. Soc. Lond. B.*, **294**: 547–588 (1981)
18. Lee, K.J., McCormick, W.D., Pearson, J.E., Swinney, H.L.: Experimental observation of self-replicating spots in a reaction-diffusion system, *Nature*, **369**(6477): 215–218 (1994)
19. Lee, K.J., Swinney, H.L.: Lamellar structures and self-replicating spots in a reaction-diffusion system, *Phys. Rev. E.*, **51**(3A): 1899–1915 (1995)
20. Lee, K.J., Swinney, H.L.: Replicating spots in reaction-diffusion systems, *Int. J. Bifurcation and Chaos*, **7**(5): 1149–1158 (1997)
21. Lyons, M.J., Harrison, L.G.: A class of reaction-diffusion mechanisms which preferentially select striped patterns, *Chem. Phys. Lett.*, **183**(1,2): 158–164 (1991)

22. Murray, J.D.: *Mathematical Biology*, Springer-Verlag, Berlin, 2nd edition, (1993)
23. Ni, W.-M.: Diffusion, cross-diffusion, and their spike-layer steady states, *Notices of the AMS.*, **45**(1): 9–18 (1998)
24. Nishiura, Y., Ueyama, D.: A skeleton structure of self-replicating dynamics, *Physica D.*, **130**: 73–104 (1999)
25. Osipov, V.V., Severtsev, A.V.: Theory of self-replication and granulation of spike autosolitons, *Phys. Lett. A.*, **222**: 400–404 (1996)
26. Painter, K.J., Maini, P.K., Othmer, H.G.: Stripe formation in juvenile *Pomacanthus* explained by a generalised Turing mechanism with chemotaxis, *Proc. Natl. Acad. Sci. USA.*, **96**: 5549–5554 (1999)
27. Pearson, J.E.: Complex patterns in a simple system, *Science.*, **261**: 189–192 (1993)
28. Petrov, V., Scott, S.K., Showalter, K.: Excitability, wave reflection, and wave splitting in a cubic autocatalysis reaction-diffusion system, *Phil. Trans. R. Soc. Lond.*, A **347**: 631–642 (1994)
29. Rasmussen, K.E., Mazin, W., Mosekilde, E.: Wave-splitting in the bistable Gray-Scott model, *Int. J. Bifurcation and Chaos.*, **6**(6): 1077–1092 (1996)
30. Reynolds, W.N., Ponce-Dawson, S., Pearson, J.E.: Self-replicating spots in reaction-diffusion systems, *Phys. Rev. E.*, **56**(1): 185–198 (1997)
31. Rinzel, J., Keller, J.B.: Travelling wave solutions of a nerve conduction equation, *Biophys. J.*, **13**: 1313–1337 (1973)
32. Schnakenberg, J.: Simple chemical reaction systems with limit cycle behaviour, *J. theor. Biol.*, **81**: 389–400 (1979)
33. Sel'kov, E.E.: Self-oscillations in glycolysis: 1. A simple kinetic model, *Eur. J. Biochem.*, **4**: 79–86 (1968)
34. Varea, C., Aragón, J.L., Barrio, R.A.: Confined Turing patterns in growing systems, *Phys. Rev. E.*, **56**(1): 1250–1253 (1997)